The Journal of Chemical Physics

The sequential activation of H_2 and N_2 mediated by the gas-phase Sc_3N^+ clusters: Formation of amido unit

Cite as: J. Chem. Phys. **154**, 054307 (2021); https://doi.org/10.1063/5.0029180
Submitted: 13 September 2020 . Accepted: 30 December 2020 . Published Online: 03 February 2021

Ming Wang, Chong-Yang Zhao, Hai-Yan Zhou, Yue Zhao, Ya-Ke Li, and Jia-Bi Ma

The Journal of Chemical Physics ARTICLE scitation.org/journal/jcp

The sequential activation of H_2 and N_2 mediated by the gas-phase Sc_3N^+ clusters: Formation of amido unit

Cite as: J. Chem. Phys. 154, 054307 (2021); doi: 10.1063/5.0029180
Submitted: 13 September 2020 • Accepted: 30 December 2020 •
Published Online: 3 February 2021

Ming Wang,[1] Chong-Yang Zhao,[1] Hai-Yan Zhou,[1] Yue Zhao,[1] Ya-Ke Li,[2,3] and Jia-Bi Ma[1,a)]

AFFILIATIONS

[1] Key Laboratory of Cluster Science of Ministry of Education, Beijing Key Laboratory of Photoelectronic/Electrophotonic Conversion Materials, School of Chemistry and Chemical Engineering, Beijing Institute of Technology, 100081 Beijing, China
[2] Wilhelm-Ostwald Institut für Physikalische und Theoretische Chemie Universität Leipzig Linnéstr. 2, 04103 Leipzig, Germany
[3] Fritz-Haber-Institut der Max-Plank-Gesellschaft, Faradayweg 4-6, 14195 Berlin, Germany

[a)] **Author to whom correspondence should be addressed:** majiabi@bit.edu.cn

ABSTRACT

The activation and hydrogenation of nitrogen are central in industry and in nature. Through a combination of mass spectrometry and quantum chemical calculations, this work reports an interesting result that scandium nitride cations Sc_3N^+ can activate sequentially H_2 and N_2, and an amido unit (NH_2) is formed based on density functional theory calculations, which is one of the inevitable intermediates in the N_2 reduction reactions. If the activation step is reversed, i.e., sequential activation of first N_2 and then H_2, the reactivity decreases dramatically. An association mechanism, prevalent in some homogeneous catalysis and enzymatic mechanisms, is adopted in these gas-phase H_2 and N_2 activation reactions mediated by Sc_3N^+ cations. The mechanistic insights are important to understand the mechanism of the conversion of H_2 and N_2 to NH_3 synthesis under ambient conditions.

INTRODUCTION

Nitrogen fixation and hydrogenation are one of the most important issues but a long-standing challenge from fundamental and practical points of view.[1,2] Both industrial and biological N_2 fixations are energy demanding.[3,4] Since the N_2 reduction reaction through $N_2 + 3H_2 \leftrightarrow 2NH_3$ is slightly thermodynamically favorable under ambient conditions, numerous efforts have been made to develop alternative and efficient processes that could produce NH_3 under more benign conditions, rather than through the energy-intensive Haber–Bosch process (450 °C and 300 bars). Mechanistic investigations indicate that in the process of N_2 reduction by H_2 over active Fe- and Ru-based catalysts, N_2 molecules are first dissociated on specific active sites (a dissociative mechanism),[5–7] and some key imido (NH) and amido (NH_2) intermediates are generated through stepwise hydrogenation,[8,9] which are usually quite stable, and therefore, elevated temperatures are needed to destabilize them.[10] It is generally agreed that co-operativity between transition metal centers is crucial for the N_2 reduction step,[11] and transition metal nitrides (TMNs) are formed in the early transition metal (such as V, Mn, and so on) catalyzed NH_3-synthesis reactions.[12,13] Some N-poor TMNs are also capable of activating N_2.[14] In addition to the early transition metals mentioned above, Ti-based, Nb-based,[15] Zr-based, W-based,[11] Mo-based,[16] and Ta-based[16,17] catalysts were applied in N_2 fixation or catalytic synthesis of ammonia. Moreover, hydrogenolysis by metal nitride intermediates is believed to be a key step in the Haber–Bosch process[18,19] and in other related processes.[20–22] Owing to their existence and importance in N_2 and H_2 activation reactions, studying the structures and reactivity of early TMNs in a molecular level remains a highly desirable and challenging target.[23] While nitrogen fixation under ambient conditions had some groundbreaking contributions in recent years, N_2 hydrogenation using dihydrogen still defines a key goal, and the detailed information on this catalytic reaction is urgently needed.

Gas-phase studies on "isolated" reactants provide an ideal arena for investigating experimentally and theoretically the possible active sites and revealing the mechanistic details of related condensed-phase systems.[24] There are some reports about the activation and cleavage of the N–N bond caused by adsorption on $Li_{2,4,6,8}$ clusters[25] and transition-metal containing clusters,[25–37] and the results indicate that the metal atom must effectively transfer electron density to the N_2 molecule to populate the π^* molecular orbitals of the molecule. Recently, Ta-related gas-phase ions, that is, Ta_2^+,[34] Ta_2N^+,[35] $Ta_2C_4^-$,[36] and $Ta_3N_3H_{0,1}^-$,[37] were capable of completely activating N_2, among which a dissociative mechanism is adopted in the reactions of N_2 with $Ta_3N_3H_{0,1}^-$ clusters.[37] In addition, the dissociative adsorption of N_2 on the $V_3C_4^-$ anion has been reported.[38] Maybe due to the lack of variations in the oxidation state, scandium and its nitrides are not a "hot choice" in N_2 fixation and activation, in comparison with the widely reported Fe-, Mo-, and other transition metal-based catalysts. Herein, we report one example about Sc_3N^+ cations on which N_2 reduction by H_2 can proceed efficiently.

METHODS

Experimental methods

The time-of-flight mass spectrometry (TOF-MS) was used to examine the ion/molecule reactions. The details of the experiments have been described in previous works,[39,40] and only a brief outline of the apparatus is given below. The ions of interest were generated by laser ablation of a scandium disk (99.999%) in 0.1% NH_3 seeded in a He carrier gas with a backing pressure of 4 atm. A 532 nm [second harmonic of Nd^{3+}:yttrium aluminum garnet (YAG)] laser with an energy of 5 mJ/pulse–8 mJ/pulse and a repetition rate of 10 Hz was used. The Sc_3N^+ ions are then mass-selected by a quadrupole mass filter (QMF) and enter into a linear ion trap (LIT) reactor, where they are confined and thermalized (see the supplementary material) by collisions with a pulse of He gas and then interact with a pulse of different kinds of reactant gases for a period of time. In our previous works,[41,42] it has been proved that the ions are thermalized to (or close to) room temperature before reactions. The ions ejected from the LIT are detected by a reflectron TOF-MS.[43]

The collision-induced dissociation (CID) experiments of Sc_3N^+ with Ar were performed, in which high center-of-mass collisional energy is added to the system under single-collision conditions. In this case, the gas Ar, rather than the cooling gas He, was delivered into the LIT reactor in which ions pass through without trapping, and to the ion source and the quadrupole mass filter were added 15 V, 26 V, and 34 V dc voltages (floating-ground mode) to increase the center-of-mass collisional energies (about 3.17 eV, 5.50 eV, and 7.20 eV, respectively). The pressure of Ar in the trap is about 780 mPa.

The photoreaction of Sc_3N^+ was studied by a TOF-MS coupled with an ultraviolet laser system. The ions were irradiated by a 355 nm laser beam (the third harmonic output of the Nd^{3+}:YAG laser) after being ejected from the LIT. The energy range of the laser is about 30 mJ/cm^2–400 mJ/cm^2 (the shot-to-shot energy stability is about ±5%). The photoreaction products and the unreacted ions passed through the reflector, and then, they were detected by a dual microchannel plate detector. The signals from the detector were recorded with a digital oscilloscope.

Computational methods

All density functional theory (DFT) calculations were performed using the Gaussian 09[44] program package employing the hybrid BPW91 exchange–correlation functional.[45,46] For all the reaction pathways, def2-QZVP[47–49] basis sets were selected for Sc atoms and 6-311+G**[50,51] for N and H atoms. The reaction mechanism calculations involve the geometry optimization of reaction intermediates and transition states (TSs). Vibrational frequency calculations were performed to ensure that the intermediates and TSs have zero and only one imaginary frequency, respectively. The intrinsic reaction coordinate (IRC) calculations[52,53] were carried out to make sure that a TS connects two appropriate minima. The reported energies (ΔH_{0K} in eV) are corrected with zero-point vibrations. Natural bond orbital (NBO) analysis was performed using NBO 6.0[54] implemented in Gaussian 09, and the program Multiwfn[55] is employed to analyze orbital compositions by the natural atomic orbital method. For the sake of clarity, the detailed information of the CCSD(T) calculations is given in the supplementary material.

RESULTS

Reactivity of Sc_3N^+ with H_2/N_2

The laser-ablation-generated Sc_3N^+ clusters were mass-selected, confined, and thermalized through collisions with helium atoms, and then, they interacted with H_2, D_2, N_2, and $^{15}N_2$. Figure 1(a) exhibits some peaks that originate from the reactions with water impurities in the LIT, and these peaks are assigned to Sc_2NO^+, $Sc_2O_2^+$, $Sc_3NO_{1,2}^+$, and $Sc_3NO_{1,2}H^+$. When the reactant gases H_2 and N_2 were injected into the reactor to react with Sc_3N^+, the adsorption product $Sc_3NH_2^+$, the secondary adsorption product $Sc_3NH_4^+$ [Reaction (1) in Table I], and $Sc_3N_3^+$ [Reaction (2)] appear, as shown in Figs. 1(b) and 1(c), respectively. The reaction of Sc_3N^+ with the mixture of N_2 and H_2 indicates that Sc_3N^+ cations are capable to adsorb both N_2 and H_2 molecules (Fig. S1 of the supplementary material). To clarify whether the sequential effect matters in these reactions, the Sc_3N^+ clusters were reacted with H_2 or N_2 seeded in the cooling gas (He) at first, and then, the other gas, which is N_2 or H_2, was pulsed into the LIT [Figs. 1(d) and 1(e)]; the different intensities of the co-adsorbate $Sc_3N_3H_2^+$ under similar reactant pressures reflect the reaction rate differences of N_2 with Sc_3N^+ and $Sc_3NH_2^+$, suggesting that the activation sequence matters. The isotopic labeling experiments with D_2 (Fig. S1 of the supplementary material), $^{15}N_2$ [Fig. 1(f)], and $D_2/^{15}N_2$ [Fig. 1(h)] were also performed. In Fig. 1(g), when D_2 was introduced into the reactor as the cooling gas, a major product corresponding to $Sc_3ND_2^+$ generates; then, upon the interaction of $^{15}N_2$ at a pressure of 0.6 Pa, the product $Sc_3N^{15}N_2D_2^+$ (m/z = 183) is obtained, as shown in Fig. 1(h), which supports the presence of the co-adsorbate $Sc_3N_3H_2^+$ rather than $Sc_3N_2O^+$.

The pseudo-first-order rate constants (k_1) for the reactions of Sc_3N^+ with reactants (H_2 and N_2) were estimated on the basis

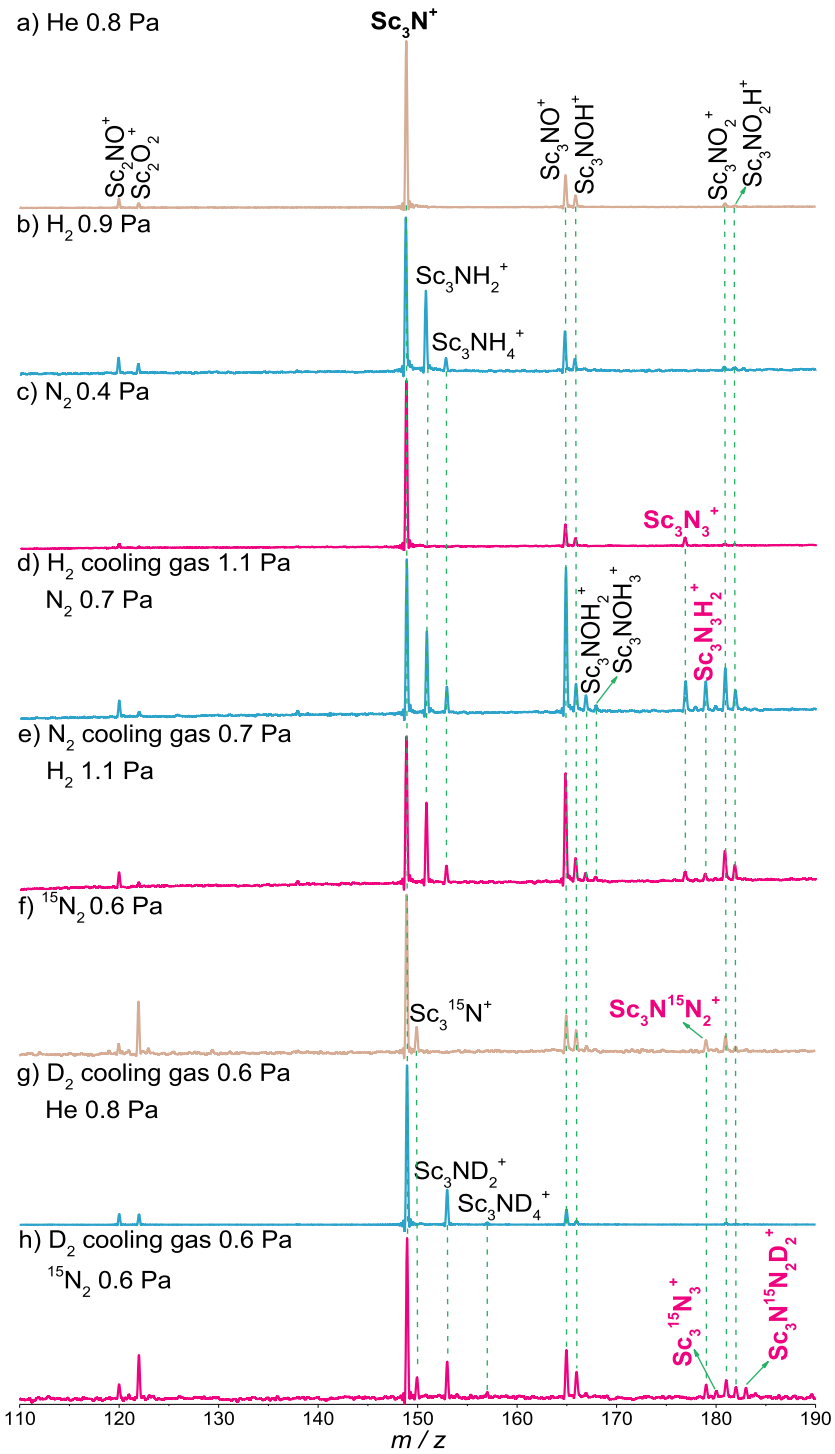

FIG. 1. Time-of-flight (TOF) mass spectra for the reactions of (a) the mass-selected Sc_3N^+ with He for 1.3 ms, (b) H_2 for 1.3 ms, (c) N_2, (d) 50% H_2 seeded in He as the cooling gas and N_2 as the reactant gas, (e) 100% N_2 as the cooling gas and H_2 as the reactant gas, (f) $^{15}N_2$, (g) 100% D_2 as the cooling gas and He as the reactant gas, and (h) 100% D_2 as the cooling gas and $^{15}N_2$ as the reaction gas. The reaction time for panels (c)–(h) is 4.0 ms. The effective reactant gas pressures are shown.

of least-squares fitting procedures (Fig. S2 of the supplementary material)[41,56] and are summarized in Table I. The $k_1(Sc_3NH_2^+ + N_2)$ is faster by about 8 times than the $k_1(Sc_3N^+ + N_2)$. Note that $Sc_3NH_2^+$ cations cannot be directly generated in our cluster source (Fig. S3 of the supplementary material). The reactivity of $ScNH^+$ and Sc_2N^+ cations toward N_2 was also investigated, and no measurable adsorption products are observed, even at a relatively high pressure of N_2 (up to 1.06 Pa) and a rather long reaction time (up to 11 ms,

TABLE I. Products, pseudo-first-order rate coefficients (k), kinetic isotope effect (KIE), and reaction efficiencies (Φ) for the reactions investigated.

No.	Reactions	k_1 (10^{-12} cm^3 molecule^{-1} s^{-1})[a]/KIE[b]	Φ (%)[c]
1	$Sc_3N^+ + H_2 \rightarrow Sc_3NH_2^+$ $Sc_3NH_2^+ + H_2 \rightarrow Sc_3NH_4^+$	$(3.6 \pm 0.7)/1.5$	0.24
2	$Sc_3N^+ + N_2 \rightarrow Sc_3N_3^+$	0.27 ± 0.06	0.04
3	$Sc_3NH_2^+ + N_2 \rightarrow Sc_3N_3H_2^+$	2.1 ± 0.4	0.32

[a]The reactant-gas-pressure-dependent experiments are shown in Fig. S2 (see the supplementary material).
[b]KIE values for reactions with dihydrogen (H_2 and D_2) are given, and these values are corrected for different collision frequencies of H_2 and D_2.
[c]$\Phi = k_1/k_{Langevin}$, where $k_{Langevin}$ is the theoretical collision rate.[57]

Fig. S4 of the supplementary material). Since the product $Sc_3N_3H_2^+$ in Fig. 1(d) can also be generated in the reaction of $Sc_3N_3^+$ with H_2, this reaction was also investigated in order to obtain its contribution. Based on the mass spectra (Fig. S5 of the supplementary material), the calculated rate constant of $Sc_3N_3^+/H_2$ is $(3.2 \pm 1.3) \times 10^{-13}$ cm^3 molecule^{-1} s^{-1}, and it is smaller than that of the $Sc_3NH_2^+/N_2$ system [$(2.1 \pm 0.4) \times 10^{-12}$ cm^3 molecule^{-1} s^{-1}]. In addition, the generation rate for $Sc_3N_3^+$ is also slow [$k_1(Sc_3N^+ + N_2 \rightarrow Sc_3N_3^+) = (2.7 \pm 0.6) \times 10^{-13}$ cm^3 molecule^{-1} s^{-1}]. Thus, it is suggested that only quite a small part of $Sc_3N_3H_2^+$ cations are generated from the reaction of $Sc_3N_3^+$ with H_2, and most of them originate from the reaction of $Sc_3NH_2^+$ with N_2.

Reaction mechanisms of Sc_3N^+ with H_2/N_2

Quantum-chemical calculations were conducted to explore the mechanistic details of the remarkable reactivity pattern. Single point CCSD(T) calculations performed at the density functional theory (DFT) optimized geometries indicate that the lowest-lying isomers of Sc_3N^+ and $Sc_3NH_2^+$ are in the doublet spin states and with C_s symmetries (^{2}**IA1** and ^{2}**IA4** in Fig. 2 and Fig. S6 of the supplementary material). In Fig. 2, all structures are pyramidal and only ^{2}**IA1** is planar. The potential energy surface (PES) of Sc_3N^+/H_2 proceeds along the doublet surface, as shown in Fig. 3(a). An H_2 molecule can be dissociated, generating an intermediate **I1** (−1.71 eV, with respect to the separated reactants). One of the H atoms is easily transferred through **TS1** and **TS2**, and $Sc_3NH_2^+$ is formed (−2.15 eV). In $Sc_3NH_2^+$, two hydrides are symmetrically bridged by the Sc atoms, and the Wiberg bond index (WBI) of the Sc–H bond is 0.4, indicating that two Sc atoms and one H atom form a three-center/two-electron (3c/2e$^-$) bond. When combined with two H atoms, the WBI values of the two Sc atoms in $Sc_3NH_2^+$ are increased by 0.4, compared to those in Sc_3N^+, and one more Sc–Sc bond is formed. Note that if the first or the second H_2 molecules are non-dissociatively adsorbed on Sc_3N^+, the adsorption energies are quite small (around 0.1 eV), which cannot be observed in the mass spectra; thus, H_2 molecules should be dissociatively adsorbed on Sc_3N^+. Furthermore, the other two isomers of Sc_3N^+ (**IA2** and **IA3**) as well as the quartet **IA1** may exist in the cluster source, and they can also react with H_2, producing $Sc_3NH_2^+$ (**P1**, Fig. S7 of the supplementary material). The major differences among **IA1**, **IA2**, and **IA3** are whether the Sc–Sc bond is formed and how long the bond lengths are.

To further investigate the structures of Sc_3N^+, the collision-induced dissociation (CID) experiments of Sc_3N^+ with Ar were also performed, in which high center-of-mass collisional energies were added to the system under single-collision conditions. As shown in Fig. 4 (see experimental methods in the supplementary material for more details), when the center-of-mass collisional energy (E_c) is 3.17 eV, one product peak Sc_2N^+ corresponding to the loss of one Sc atom formed. The DFT calculated bond dissociation energy for $[Sc–Sc_2N]^+$ is 2.95 eV (**IA1**, see Table S1), which is close to the CID result. Since the product $Sc_3NH_2^+$ or the co-adsorbate $Sc_3N_3H_2^+$ cannot be selected in our apparatus, the CID experiments of these clusters with Ar cannot be conducted. Photo-induced dissociation (PID) experiments at 355 nm have also been carried out to get more structure information. In the laser-on experiments of the products $Sc_3NH_2^+$ and $Sc_3NH_4^+$ [Figs. 4(b) and S9], their relative intensities

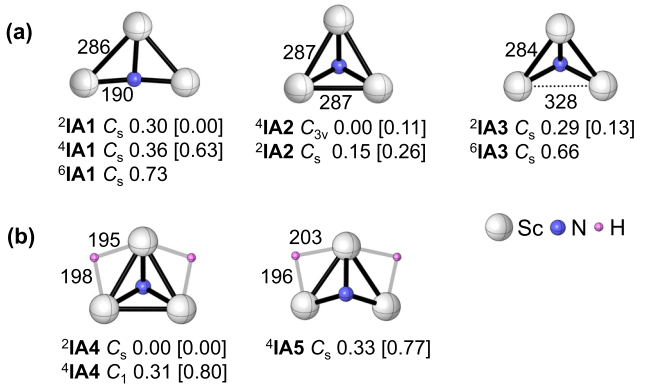

^{2}**IA1** C_s 0.30 [0.00]
^{4}**IA1** C_s 0.36 [0.63]
^{6}**IA1** C_s 0.73
^{4}**IA2** C_{3v} 0.00 [0.11]
^{2}**IA2** C_s 0.15 [0.26]
^{2}**IA3** C_s 0.29 [0.13]
^{6}**IA3** C_s 0.66
^{2}**IA4** C_s 0.00 [0.00]
^{4}**IA4** C_1 0.31 [0.80]
^{4}**IA5** C_s 0.33 [0.77]

FIG. 2. DFT-calculated structures and relative energies of (a) Sc_3N^+ and (b) $Sc3NH_2^+$. Relative energies by CCSD(T) are given in square brackets. The point group is given under each structure. Bond lengths are given in pm. The superscripts indicate the spin states.

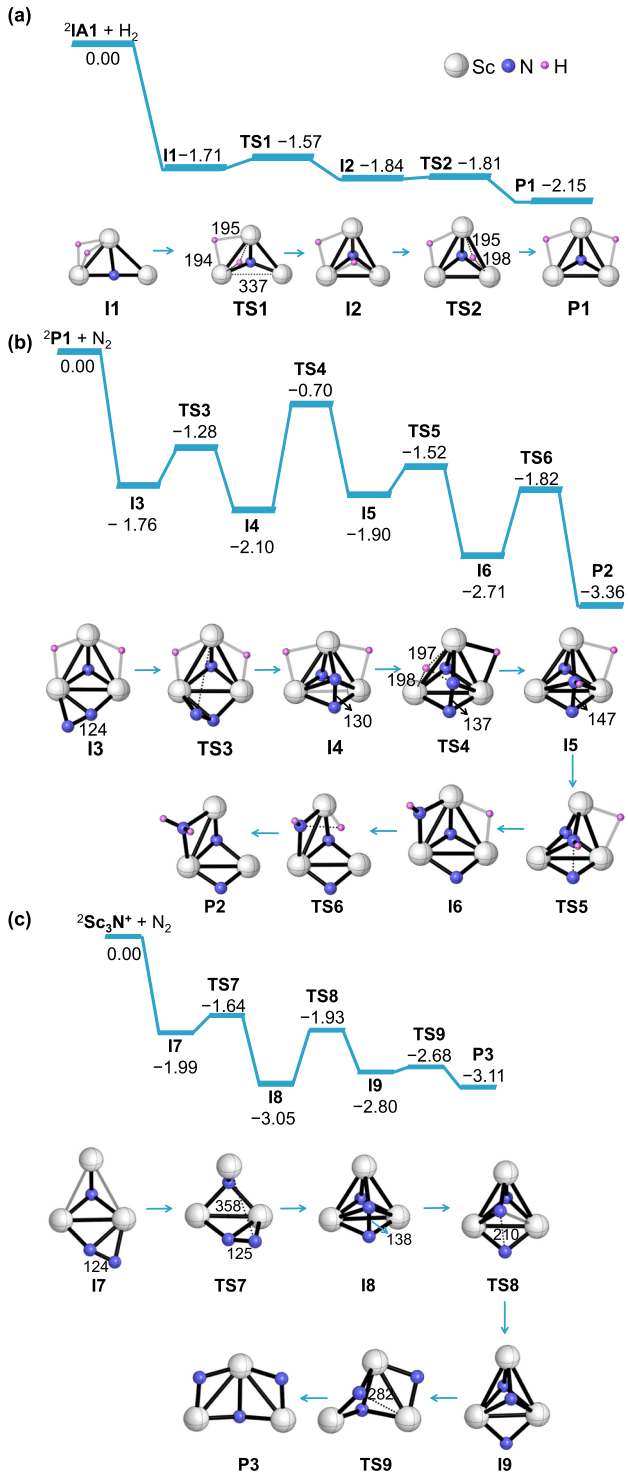

FIG. 3. DFT-calculated potential energy surfaces for the reactions of (a) Sc_3N^+ (^{2}**IA1**) with H_2, (b) $Sc_3NH_2^+$ with N_2, and (c) Sc_3N^+ (^{2}**IA1**) with N_2. Some bond lengths are given in pm. The zero-point vibration corrected energies (ΔH_{0K} in eV) of the reaction intermediates, transition states, and products with respect to the separated reactants are given.

decrease while those of the reactant Sc_3N^+ increase as increasing the laser fluences; no hydrogen atom loss product or $Sc_2NH_2^+$ is observed. According to the DFT calculations, the H_2 losses from $Sc_3NH_2^+$ and $Sc_3NH_4^+$ to generate Sc_3N^+ and $Sc_3NH_2^+$ are 2.15 eV and 1.57 eV, respectively; the lowest energies for one H loss from $Sc_3NH_2^+$ and $Sc_3NH_4^+$ are 3.15 eV and 2.63 eV, respectively. In this case, H_2 is much easier to be released than the H atom in both hydrogenated clusters. The experiments of structure characterization also indicate that the DFT calculation results are reliable.

As shown in Fig. 3(b), the DFT calculations predict that dinitrogen approaches the $Sc_3NH_2^+$ clusters through side-on (η^1) and side-on/end-on dinuclear (η^1:η^2) modes; the first mode can transform into the much more stable η^1:η^2-N_2 mode through two transition states [Fig. S10(a) of the supplementary material]. Through **TS3**, two more Sc–N bonds are formed in **I4**, and the N–N bond length is elongated by 20 pm, compared with the free N_2 molecule (110 pm). In **I4**, N_2 is coordinated with three Sc atoms in the side-on/side-on/end-on configuration (μ_3-η^2:η^2:η^1) based on the bonding modes structurally characterized in the solid states.[43] This coordination mode has been reported in the $V_3C_4^-/N_2$ system.[38] During the next step, one of the hydride atoms transfers to the near N atom in the N_2 unit through **TS4**, concomitant with the increasing N–N bond from 130 pm in **I4** to 147 pm in **I5**. The NN bond is finally broken through **TS5**, leading to the formation of one NH unit in **I6**; then, the other hydrogen migrates to this NH moiety and generates the NH_2 unit as the product **P2**. **TS4** is a relatively high barrier, but **P2** is much more stable than **I4** in energy (−3.36 eV vs −2.10 eV), providing the thermodynamic driving force. The Rice–Ramsberger–Kassel–Marcus (RRKM) theory[58] is employed to estimate the absolute rate constant ($k_{conversion}$) of the traversing transition state **TS4** from intermediate **I4** (a detailed description is given in the supplementary material). The calculated $k_{conversion}$ for **I4** → **TS4** is 1.8×10^8 s^{-1}, which is three orders of magnitude faster than the rate (5.5×10^5 s^{-1}) of collisions between **I4** and the bath gas He. Therefore, most of **I4** can still overcome **TS4** to generate **P2**. Notably, the complete activation of the NN bond rather than overcoming **TS4** from **I4** is not achievable (Fig. S11 of the supplementary material). We also calculate the PES of Sc_3N^+/N_2, shown in Fig. 3(c), and the reaction occurs via a dissociative mechanism. Since the product of $Sc_3N_3^+$ (**P3**) and the intermediate **I8** with the μ_3-η^2:η^2:η^1-N_2 mode are comparable in energy, a high barrier is involved; thus, most of the experimentally observed $Sc_3N_3^+$ should be adsorption products **I8**. The product energy of the $Sc_3NH_2^+/N_2$ system (−3.36 eV) is more favorable than that of Sc_3N^+/H_2 (−3.11 eV). In addition, the secondary adsorption product $Sc_3NH_4^+$ can also adsorb one N_2 molecule, but according to the DFT calculations, that N_2 should be the physically adsorbed, rather than dissociatively adsorbed (Fig. S12).

To further understand the faster reaction rate of $Sc_3NH_2^+ + N_2$ compared to that of $Sc_3N^+ + N_2$, the potential energy curves to form **I3** and **I7** were carefully followed. In Fig. S13, the hydrogenated cluster has a relatively deeper entrance channel to form the encounter complex than the $Sc_3N^+ + N_2$ system. Since there are also η^1 adsorption modes of the first complexes $Sc_3NH_{0,2}^+ \ldots N_2$, more calculations considering the transformation between these structures and the values of $k_{conversion}$ from adsorption intermediates as well as the dissociation rates (k_d) of N_2 desorption from these encounter complexes based on an RRKM-based variational transition state theory

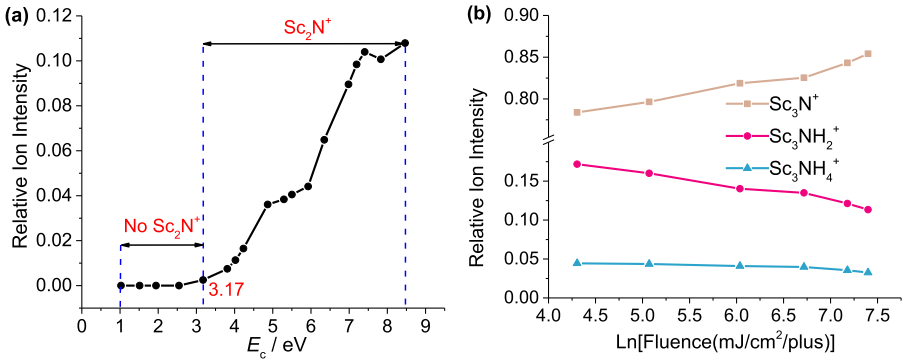

FIG. 4. (a) The relative ion intensity of Sc_2N^+ with respect to E_c. (b) Experimental ion intensity of reactant and product clusters ($Sc_3NH_{0,2,4}^+$) for the photo-induced dissociation under different laser fluences.

(VTST) approach[59] are also performed. As shown in Fig. S10(b), for the adducts with η^1-N_2 modes in $Sc_3NH_2^+$, $k_{conversion}$ (10^{10} s^{-1}) is one order of magnitude faster than k_d. In contrast, $k_{conversion}$ (1.4×10^{11} s^{-1}) is slightly slower than k_d (4.5×10^{11} s^{-1}) in the Sc_3N^+/N_2 system. Thus, when N_2 molecules are adsorbed on clusters via the η^1 mode, $Sc_3NH_2^+$ should react more efficiently than Sc_3N^+. Taking all these factors into account, $Sc_3NH_2^+$ has higher reactivity toward N_2 than the dehydrogenated Sc_3N^+, in line with the experimental findings. In addition, the infrared spectrometry of $Sc_3N_3H_2^+$ is given in the supplementary material. The vibrational frequencies may be used for future experimental identification of these clusters.

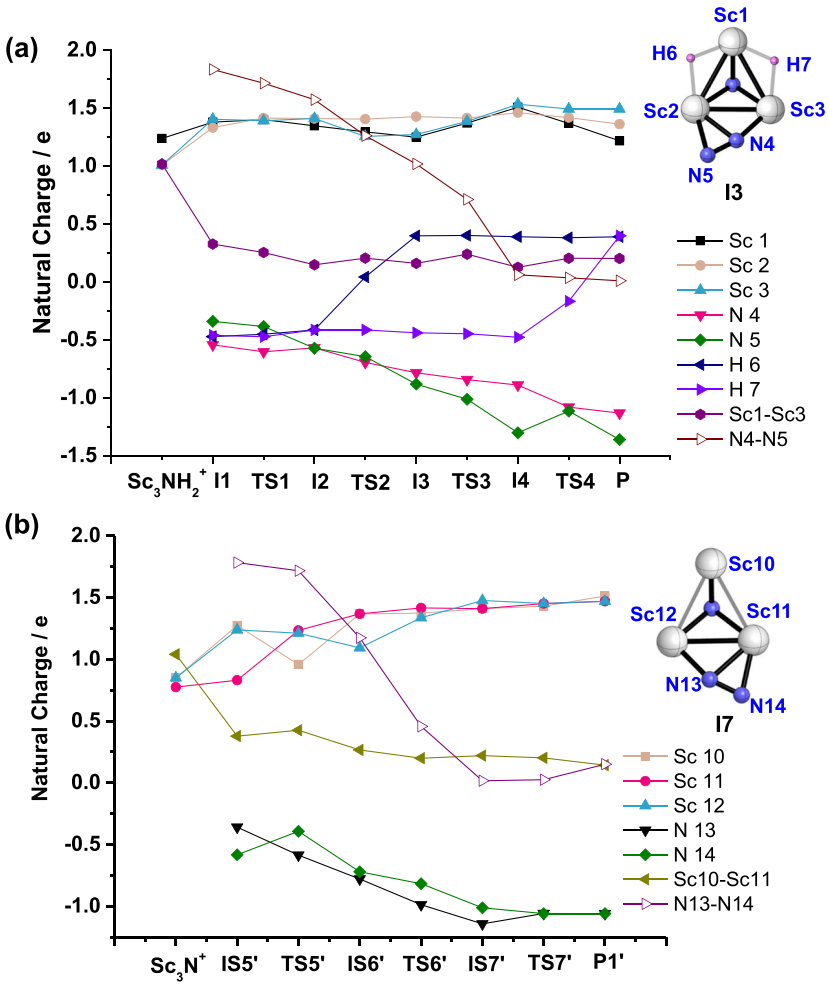

FIG. 5. Charges on atoms of stationary points along reaction coordinates of N_2 activation on (a) $Sc_3NH_2^+$ and (b) Sc_3N^+ clusters. The hollow triangles represent bond orders of N_2 units. Some atoms are labeled and shown in the right panel.

DISCUSSION

Natural bond orbital analysis indicates that the electrons used to reduce N_2 molecules stem from different atoms in Sc_3N^+ and $Sc_3NH_2^+$ clusters. As shown in Fig. 5, the electron donors in Sc_3N^+ and $Sc_3NH_2^+$ are three Sc atoms and two hydrogen atoms, respectively, during the reactions with N_2. The dihydrogen herein acts both as the proton and electron sources for N_2 reduction mediated by $Sc_3NH_2^+$. In addition, the WBI of the Sc–Sc bond decreases from 1 in $Sc_3NH_2^+$ to 0.33 in **I3** and the NN bond of N_2 is elongated, indicating that two electrons are ejected into the N_2 molecule from $Sc_3NH_2^+$. Counting the four electrons provided by the two H^- atoms, there are totally six electrons transferred from $Sc_3NH_2^+$ to N_2, and N_2 is reduced into N^{3-} ions. For **TS4** and **TS6** in Fig. 3(b), hydride transfer processes are identified. Since the nitrogen atoms, hydride acceptors, also carry negative charges, an energy-demanding transition state **TS4** is encountered in the PES, which accounts for the rate-limiting step.

The proposed reaction mechanism of reductive N_2 activation to form the amido unit (NH_2) in $Sc_3NH_2^+$ is to first weaken the NN bond in N_2 by adding one H atom, generating the *NNH-like intermediate **I5** (the asterisk * denotes an adsorption site), and *NNH is further activated through the complete breakage of the NN bond. In the Haber–Bosch process, the N≡N bond is first dissociated on specific active sites, and then, the adsorbed *N is hydrogenated step by step to produce $^*NH_3$, which is a dissociative mechanism. In contrast, associative adsorption or hydrogenation of N_2, an association mechanism, is prevalent in some homogeneous catalysis and enzymatic mechanisms.[60,61] In these reactions that followed the association mechanism under thermochemical conditions, the elementary steps involved are as follows:[60,62]

$$^*N_2 + {}^*H \rightarrow {}^*NNH + {}^*, \tag{4}$$

$$^*NNH \rightarrow {}^*N + {}^*NH, \tag{5}$$

$$^*NH + H^+ + e^- \rightarrow {}^*NH_2. \tag{6}$$

The reaction of $Sc_3NH_2^+$ with N_2 shown in Fig. 3(b) also proceeds based on this associative mechanism. Reactions (4)–(6) correspond to **I4** → **I5**, **I5** → **I6**, and **I6** → **P2** steps, respectively. The most energy-demanding step is the first hydrogenation of $^*N_2$. It is also consistent with the fact that in the electrochemical ammonia synthesis, *NNH formation by hydrogenolysis is the potential-determining step.[63,64] It is noteworthy that in gas-phase studies, sequential activation of two kinds of molecules has been reported, such as $Re(CO)_2^+/CO_2/CH_4$ and $CuB^+/CH_4/CO_2$ systems,[65,66] and in these reactions, the sequence of events matters.

CONCLUSIONS

In summary, the sequential thermal reactions of the Sc_3N^+ cations with H_2 and N_2 have been investigated by using mass spectrometry and quantum-chemical calculations. The reaction rate of $Sc_3NH_2^+$, generated from the hydrogenation reaction of Sc_3N^+ with H_2, is about 8 times faster than that of the N_2/Sc_3N^+ system; thus, the sequence of events matters. Through reliable DFT calculations, the NH_2 unit is formed in the N_2 hydrogenation reactions. Along the whole potential energy surface, the rate-limiting step is the first hydrogenation of the adsorbed N_2 molecule, and six electrons (two from the Sc–Sc bond and four from the two H^- atoms) in $Sc_3NH_2^+$ are transferred into the N_2 molecule to generate two N^{3-} ions. The associative mechanism, prevalent in some homogeneous catalysis and enzymatic systems, is also followed in the gas-phase reactions of $Sc_3NH_2^+$ with N_2. Ideal catalysts that allow energy-efficient NH_3 synthesis should activate N_2 well but bind intermediates, such as amido and imido, relatively weakly. Our gas-phase model systems show the fundamental mechanisms behind the important issue of N_2 fixation and hydrogenation, and studies on modified scandium nitride clusters that may bind the NH_2 unit more weakly are in progress.

SUPPLEMENTARY MATERIAL

See the supplementary material for the additional time-of-flight (TOF) mass spectra results, the method of determining the rate constants, the additional density functional theory results, the additional experimental results of collision-induced dissociation (CID) and photo-induced dissociation (PID), the methods for the determination of the collision rates of key intermediates with the cooling gas He ($k_{collision}$) and the conversion rates ($k_{conversion}$) of some key steps as well as the rates for N_2 desorption from intermediates, the additional theoretical results of the CCSD(T) calculations, and the IR spectrum of $Sc_3N_3H_2^+$.

ACKNOWLEDGMENTS

This work was supported by the National Natural Science Foundation of China (Grant Nos. 91961122 and 21833011), the National Key R&D Program of China (Grant No. 2016YFC0203000), and the Fundamental Research Funds for the Central Universities (Grant No. 2017CX01008). Y.-K. Li thanks the Alexander von Humboldt Foundation for a post-doctoral research fellowship.

DATA AVAILABILITY

The data that support the findings of this study are available within the article and its supplementary material.

REFERENCES

[1] M. D. Fryzuk and S. A. Johnson, Coord. Chem. Rev. **200–202**, 379 (2000).
[2] D. V. Yandulov and R. R. Schrock, Science **301**, 76 (2003).
[3] J. W. Erisman, M. A. Sutton, J. Galloway, Z. Klimont, and W. Winiwarter, Nat. Geosci. **1**, 636 (2008).
[4] B. K. Burgess and D. J. Lowe, Chem. Rev. **96**, 2983 (1996).
[5] K. Honkala, A. Hellman, I. N. Remediakis, A. Logadottir, A. Carlsson, S. Dahl, C. H. Christensen, and J. K. Norskov, Science **307**, 555 (2005).
[6] D. R. Strongin, J. Carrazza, S. R. Bare, and G. A. Somorjai, J. Catal. **103**, 213 (1987).

[7]K. Reuter, C. P. Plaisance, H. Oberhofer, and M. Andersen, J. Chem. Phys. **146**, 040901 (2017).
[8]C. J. M. Van der Ham, M. T. M. Koper, and D. G. H. Hetterscheid, Chem. Soc. Rev. **43**, 5183 (2014).
[9]P. Avenier, M. Taoufik, A. Lesage, X. Solans-Monfort, A. Baudouin, A. de Mallmann, L. Veyre, J.-M. Basset, O. Eisenstein, L. Emsley, and E. A. Quadrelli, Science **317**, 1056 (2007).
[10]J. K. Norskov, T. Bligaard, J. Rossmeisl, and C. H. Christensen, Nat. Chem. **1**, 37 (2009).
[11]S. Gambarotta and J. Scott, Angew. Chem., Int. Ed. **36**, 5298 (2005).
[12]D. A. King and F. Sebba, J. Catal. **4**, 253 (1965).
[13]A. Mittasch and W. Frankenburg, Adv. Catal. **2**, 81 (1950).
[14]P. Wang, F. Chang, W. Gao, J. Guo, G. Wu, T. He, and P. Chen, Nat. Chem. **9**, 64 (2017).
[15]A. E. Shilov, Russ. Chem. Bull. **52**, 2555 (2003).
[16]H. Tanaka, Y. Nishibayashi, and K. Yoshizawa, Acc. Chem. Res. **49**, 987 (2016).
[17]Y. Kobayashi, Y. Tang, T. Kageyama, H. Yamashita, N. Masuda, S. Hosokawa, and H. Kageyama, J. Am. Chem. Soc. **139**, 18240 (2017).
[18]R. Schlögl, Angew. Chem., Int. Ed. **42**, 2004 (2003).
[19]H.-P. Jia and E. A. Quadrelli, Chem. Soc. Rev. **43**, 547 (2014).
[20]B. Askevold, J. T. Nieto, S. Tussupbayev, M. Diefenbach, E. Herdtweck, M. C. Holthausen, and S. Schneider, Nat. Chem. **3**, 532 (2011).
[21]D. Bao, Q. Zhang, F.-L. Meng, H.-X. Zhong, M.-M. Shi, Y. Zhang, J.-M. Yan, Q. Jiang, and X.-B Zhang, Adv. Mater. **29**, 1604799 (2017).
[22]S. D. Brown, M. P. Mehn, and J. C. Peters, J. Am. Chem. Soc. **127**, 13146 (2005).
[23]J. Schöffel, A. Y. Rogachev, S. D. George, and P. Burger, Angew. Chem., Int. Ed. **48**, 4734 (2009).
[24]L.-X. Jiang, C. Zhao, X.-N. Li, H. Chen, and S.-G. He, Angew. Chem., Int. Ed. **56**, 4187 (2017).
[25]D. Roy, A. Navarro-Vazquez, and P. V. R. Schleyer, J. Am. Chem. Soc. **131**, 13045 (2009).
[26]M. M. Doeff, S. F. Parker, P. H. Barrett, and R. G. Pearson, Inorg. Chem. **23**, 4108 (1984).
[27]K. N. Shrivastava, S. S. C. Ammal, H. Tsuruya, S. Takami, A. Endou, M. Kubo, K. Teraishi, A. Miyamoto, and A. Ozaki, Chem. Phys. Lett. **313**, 279 (1999).
[28]Z. Cao, H. Wan, and Q. Zhang, J. Chem. Phys. **119**, 9178 (2003).
[29]Z.-H. Lu, L. Jiang, and Q. Xu, J. Phys. Chem. A **114**, 6837 (2010).
[30]C. Kerpal, D. J. Harding, J. T. Lyon, G. Meijer, and A. Fielicke, J. Phys. Chem. C **117**, 12153 (2013).
[31]H. C. Heim, T. M. Bernhardt, S. M. Lang, R. N. Barnett, and U. Landman, J. Phys. Chem. C **120**, 12549 (2016).
[32]F. Mafuné, Y. Tawaraya, and S. Kudoh, J. Phys. Chem. A **120**, 4089 (2016).
[33]H.-J. Himmel and M. Reiher, Angew. Chem., Int. Ed. **45**, 6264 (2006).
[34]C. Geng, J. Li, T. Weiske, and H. Schwarz, Proc. Natl. Acad. Sci. U. S. A. **115**, 11680 (2018).
[35]C.-Y. Geng, J.-L. Li, T. Weiske, and H. Schwarz, Proc. Natl. Acad. Sci. U. S. A. **116**, 21416 (2018).
[36]Z.-Y. Li, L.-H. Mou, G.-P. Wei, Y. Ren, M.-Q. Zhang, Q.-Y. Liu, and S.-G. He, Inorg. Chem. **58**, 4701 (2019).
[37]Y. Zhao, J.-T. Cui, M. Wang, D. Y. Valdivielso, A. Fielicke, L.-R. Hu, X. Cheng, Q.-Y. Liu, Z.-Y. Li, S.-G. He, and J.-B. Ma, J. Am. Chem. Soc. **141**, 12592 (2019).
[38]Z.-Y. Li, Y. Li, L.-H. Mou, J.-J. Chen, Q.-Y. Liu, S.-G. He, and H. Chen, J. Am. Chem. Soc. **142**, 10747 (2020).
[39]X.-N. Wu, B. Xu, J.-H. Meng, and S.-G. He, Int. J. Mass Spectrom. **310**, 57 (2012).
[40]Z. Yuan, Y.-X. Zhao, X.-N. Li, and S.-G. He, Int. J. Mass Spectrom. **354-355**, 105 (2013).
[41]Z. Yuan, Z.-Y. Li, Z.-X. Zhou, Q.-Y. Liu, Y.-X. Zhao, and S.-G. He, J. Phys. Chem. C **118**, 14967 (2014).
[42]Y.-X. Zhao, Z.-Y. Li, Z. Yuan, X.-N. Li, and S.-G. He, Angew. Chem., Int. Ed. **53**, 9482 (2014).
[43]Z.-Y. Li, Z. Yuan, X.-N. Li, Y.-X. Zhao, and S.-G. He, J. Am. Chem. Soc. **136**, 14307 (2014).
[44]M. J. Frisch, G. W. Trucks, H. B. Schlegel, G. E. Scuseria, M. A. Robb, J. R. Cheeseman, G. Scalmani, V. Barone, B. Mennucci, G. A. Petersson, H. Nakatsuji, M. Caricato, X. Li, H. P. Hratchian, A. F. Izmaylov, J. Bloino, G. Zheng, J. L. Sonnenberg, M. Hada, M. Ehara, K. Toyota, R. Fukuda, J. Hasegawa, M. Ishida, T. Nakajima, Y. Honda, O. Kitao, H. Nakai, T. Vreven, Jr., J. A. Montgomery, J. E. Peralta, F. Ogliaro, M. Bearpark, J. J. Heyd, E. Brothers, K. N. Kudin, V. N. Staroverov, T. Keith, R. Kobayashi, J. Normand, K. Raghavachari, A. Rendell, J. C. Burant, S. S. Iyengar, J. Tomasi, M. Cossi, N. Rega, J. M. Millam, M. Klene, J. E. Knox, J. B. Cross, V. Bakken, C. Adamo, J. Jaramillo, R. Gomperts, R. E. Stratmann, O. Yazyev, A. J. Austin, R. Cammi, C. Pomelli, J. W. Ochterski, R. L. Martin, K. Morokuma, V. G. Zakrzewski, G. A. Voth, P. Salvador, J. J. Dannenberg, S. Dapprich, A. D. Daniels, O. Farkas, J. B. Foresman, J. V. Ortiz, J. Cioslowski, and D. J. Fox, Gaussian 09, Revision D.01, Gaussian, Inc., Wallingford, CT, 2013.
[45]J. P. Perdew and Y. Wang, Phys. Rev. B **45**, 13244 (1991).
[46]J. P. Perdew, J. A. Chevary, S. H. Vosko, K. A. Jackson, M. R. Pederson, D. J. Singh, and C. Fiolhais, Phys. Rev. B **46**, 6671 (1992).
[47]D. Andrae, U. Haussermann, M. Dolg, H. Stoll, and H. Preuss, Theor. Chim. Acta **77**, 123 (1990).
[48]B. Metz, H. Stoll, and M. Dolg, J. Chem. Phys. **113**, 2563 (2000).
[49]T. Leininger, A. Nicklass, W. Küchle, H. Stoll, M. Dolg, and A. Bergner, Chem. Phys. Lett. **255**, 274 (1996).
[50]T. Clark, J. Chandrasekhar, G. W. Spitznagel, and P. V. R. Schleyer, J. Comput. Chem. **4**, 294 (1983).
[51]R. Krishnan, J. S. Binkley, R. Seeger, and J. A. Pople, J. Chem. Phys. **72**, 650 (1980).
[52]C. Gonzalez and H. B. Schlegel, J. Chem. Phys. **90**, 2154 (1989).
[53]C. Gonzalez and H. B. Schlegel, J. Phys. Chem. **94**, 5523 (1990).
[54]E. D. Glendening, J. K. Badenhoop, A. E. Reed, J. E. Carpenter, J. A. Bohmann, C. M. Morales, C. R. Landis, and F. Weinhold, NBO 6.0, Theoretical Chemistry Institute, University of Wisconsin, Madison, WI, 2013, http://nbo6.chem.wisc.edu/.
[55]T. Lu and F. Chen, J. Comput. Chem. **33**, 580 (2012).
[56]X.-N. Li, Z. Yuan, and S.-G. He, J. Am. Chem. Soc. **136**, 3617 (2014).
[57]P. Langevin, Ann. Chim. Phys. **5**, 245 (1905).
[58]J. I. Steinfeld, J. S. Francisco, and W. L. Hase, *Chemical Kinetics and Dynamics* (Prentice-Hall, Upper Saddle River, New Jersey, 1999), p. 231.
[59]J. I. Steinfeld, J. S. Francisco, and W. L. Hase, *Chemical Kinetics and Dynamics* (Prentice-Hall, Upper Saddle River, New Jersey, 1999), pp. 313–314.
[60]J. S. Anderson, J. Rittle, and J. C. Peters, Nature **501**, 84 (2013).
[61]I. Coric and P. L. Holland, J. Am. Chem. Soc. **138**, 7200 (2016).
[62]S. E. Creutz and J. C. Peters, J. Am. Chem. Soc. **136**, 1105 (2014).
[63]J. H. Montoya, C. Tsai, A. Vojvodic, and J. K. Nørskov, Chemsuschem **8**, 2180 (2015).
[64]Y.-C. Hao, Y. Guo, L.-W. Chen, M. Shu, X.-Y. Wang, T.-A. Bu, W.-Y. Gao, N. Zhang, X. Su, X. Feng, J.-W. Zhou, B. Wang, C.-W. Hu, A.-X. Yin, R. Si, Y.-W. Zhang, and C.-H. Yan, Nat. Catal. **2**, 448 (2019).
[65]S. Zhou, J. Li, M. Firouzbakht, M. Schlangen, and H. Schwarz, J. Am. Chem. Soc. **139**, 6169 (2017).
[66]Q. Chen, Y.-X. Zhao, L.-X. Jiang, J.-J. Chen, and S.-G. He, Angew. Chem., Int. Ed. **57**, 14134 (2018).